Biosensors and Bioelectronics 30 (2011) 21–27

Contents lists available at SciVerse ScienceDirect

Biosensors and Bioelectronics

journal homepage: www.elsevier.com/locate/bios

A label-free optical sensor based on nanoporous gold arrays for the detection of oligodeoxynucleotides

Jiandong Feng, Weijie Zhao, Bin Su**, Jianmin Wu*

Institute of Microanalytical System, Department of Chemistry, Zhejiang University, Hangzhou 310058, China

ARTICLE INFO

Article history:
Received 5 June 2011
Received in revised form 16 August 2011
Accepted 16 August 2011
Available online 25 August 2011

Keywords:
Nanoporous gold
Porous silicon
Label free
Optical biosensor
Oligonucleotides

ABSTRACT

Interest in using nanoporous materials for sensing applications has increased. The present study reports a method of preparing well-ordered nanoporous gold arrays using a porous silicon (PSi) template. Gold nanolayer could be electrodeposited on the surface of the PSi template at low electrolysis currents in low concentration of chloroauric acid ($HAuCl_4$) solution. Surface morphology characterizations and optical measurements revealed that a PSi-templated nanoporous gold (Au–PSi) array well replicated the nanoporous structure and retained the optical properties of PSi. Fourier transform reflectometric interference spectra showed that a characteristic blue-shifted effective optical thickness (EOT) was observed due to the low refractive index of the gold film. An optical DNA biosensor was then fabricated via the self-assembly of single-stranded DNA (ssDNA) with a specific sequence on the surface of Au–PSi. The attachment of ssDNA and its hybridization with target oligonucleotides (ODNs) persistently caused the blue shift of the EOT. Consequently, a relationship between the EOT shift and the ODN concentration was established. The mechanism of the optical response caused by DNA hybridization on the Au–PSi surface was qualitatively explained by the electromagnetic theory and electrochemical impedance spectroscopy (EIS). The lowest detection limit for target ODNs was estimated at around 10^{-14} mol L^{-1}, when the baseline noise, a variation in the value of EOT is around 5 nm. The fabricated Au–PSi based optical biosensor has potential use in the discovery of new ODN drugs because it will be able to detect the binding event between ODNs and the target DNA.

1. Introduction

Nanoporous materials have attracted much attention for label-free sensing applications. These materials have the advantages of a large available surface area for molecular binding, as well as a capability for size-selective molecule filtering and sensing (Kececi et al., 2008; Lin et al., 1997; Martin and Siwy, 2007). Among various nanoporous materials, porous silicon (PSi) is one of the most suitable sensing candidates (Cunin et al., 2002; Dancil et al., 1999; Lin et al., 1997). PSi layers can be easily produced on single-crystal Si substrates by a simple electro-anodization process in an HF-containing electrolyte. A wide range of pore morphologies can be repeatedly obtained by a simple manipulation of the electrical etching conditions. Such conditions include the substrate doping type and level, HF concentration in the electrolyte, as well as anodization current density. Molecular binding events in porous layers can be detected by monitoring interference patterns using reflectance spectroscopy (Lin et al., 1997), an angle-resolved reflectance waveguide (Chan et al., 2001; Rong et al., 2008a,b), or optical resonant microcavity (Chan et al., 2001).

DNA hybridization is one of the most important molecular binding events in biomedical research. Hence, observing the DNA hybridization signal plays a vital role in gene detection and drug discovery. Research on PSi optical sensors for detecting DNA hybridization has been reported (Lin et al., 1997; Rong et al., 2008b). However, biosensing materials based on PSi still has some evident defects, such as degradation and instability in a buffer solution (van Noort and Mandenius, 2000). Attempts have been made to overcome the instability of silicon surface. For example, the formation of a SiO_2 surface layer via the oxidation of PSi at high temperatures or with ozone treatment can relatively improve the stability of the porous Si sensing layer. Another method is to deposit a gold nanolayer on PSi (Garcia-Maldonado et al., 2005; Hong et al., 2010), as have also been done for porous polymeric membranes (Wirtz and Martin, 2003). Apart from retaining the porous structure of PSi, a gold layer also has a high chemical stability and electronic conductivity, as well as surface properties that can be tailored by a variety of self-assembled monolayers via thiol chemistry. Therefore, nanoporous gold arrays produced by the deposition of gold atoms on PSi templates are potential candidate materials for constructing optical or electrochemical biosensors.

* Corresponding author. Tel.: +86 571 88273496; fax: +86 571 88273572.
** Co-corresponding author.
E-mail addresses: subin@zju.edu.cn (B. Su), wjm-st1@zju.edu.cn (J. Wu).

0956-5663/$ – see front matter © 2011 Elsevier B.V. All rights reserved.
doi:10.1016/j.bios.2011.08.021

In the current work, well-ordered porous Au nanostructures were prepared by the electrodeposition of gold atoms on a PSi template. The Au nanostructures could almost replicate the PSi structure comprising pore arrays after the electrodeposition, except that the average pore diameter of the Au nanostructures reduced. Hence, PSi-templated nanoporous gold arrays (Au–PSi) were obtained. Subsequently, a kind of optical Au–PSi DNA sensor was conveniently fabricated by attaching a capture probe, 5′-thiolated single-strand DNA (ssDNA), on the Au–PSi surface via self-assembly. Target oligodeoxynucleotide (ODN) molecules with sequences complementary to the probe ssDNA specifically bound with the Au–PSi surface. This binding caused a change in the refractive index of the porous Au–PSi layer. ODN detection was simply realized by monitoring the shift in the effective optical thickness (EOT) of the Au–PSi layer. This shift was detected by Fourier transform reflectometric interference spectra (FT-RIFS). For ODN detection, the Au–PSi based DNA sensor displayed a key advantage over others owing to the size filtering effect of the nanoporous structure.

Antisense ODNs have been reported to offer a great potential in regulating the expression of specific genes within cells (Stein and Cohen, 1988). Observing the binding event between antisense ODNs and the target gene may lead to the discovery of new therapies for human diseases. The size selectivity and optical properties of the Au–PSi sensor will enable its potential applications in studying molecular interactions between these ODN drugs and target genes.

2. Material and methods

2.1. Preparation and characterization of Au–PSi

PSi was prepared by the electrochemical etching of single-crystal Si wafers in a two-electrode configuration using a platinum mesh counter-electrode. Si wafers (P++, 0.1 mΩ cm, Siltronix Co., France) with an exposed area of 1.2 cm^2 were contacted on the back side with a strip of aluminum foil and mounted in a Teflon etching cell. The aluminum foil and Si wafer is placed in a PTE electrolysis vessel, and the etching area was defined by an O-ring. Prior to electrochemical etching, the wafers were sonicated in acetone and rinsed with ultrapure water. Electrochemical etching was performed at a constant current of 30 mA for 450 s in electrolyte mixture solution of HF (49%) and ethanol (3:1, v/v). An NJ-320 potentiostat/galvanostat (Najing Scientific Instrumental Co., Xiamen, China) was used as the current source. The etching current was controlled using a homemade computer software. After etching, the samples were thoroughly rinsed with ethanol and dried in a nitrogen gas flow.

A layer of gold film was electrochemically deposited on the obtained PSi wafer in the same PTE electrolysis vessel. The PSi and platinum counter electrodes acted as the cathode and anode, respectively. The PTE electrolysis vessel was filled with a solution of 0.001% $HAuCl_4$, and electrodeposition was performed at a constant current of 5 mA for 10 min. The resulting Au–PSi was rinsed with distilled water and ethanol prior to use.

The surface and cross-sectional morphology of PSi with and without gold plating was compared by microscopic measurements via scanning electron microscopy (SEM; SIRON field emission scanning electron microscope, FEI Corp., Netherlands) at an accelerating voltage of 10 keV in the secondary electron imaging mode.

2.2. Reflectance spectra of the porous films

Reflectance spectra were obtained on a USB 4000 miniaturized fiber spectrophotometer (Ocean Optics, USA). An LS-1 halogen tungsten lamp was used as the light source to illuminate the surface of Au–PSi through one arm of a bifurcated fiber optic cable at normal incidence with a focused spot size of approximately 2 mm^2. The reflected light covering the wavelength range of 400–1000 nm was transmitted through another arm of the bifurcated fiber, and was collected by the Spectrasuit software (Ocean Optics) with an integration time of 100 ms. The EOT was determined from the Fabry–Pérot relationship:

$$2nL = m\lambda \quad (1)$$

where λ is the wavelength of maximum constructive interference for a spectral fringe of order m, n is the average refractive index of the porous layer and its contents, and L is the thickness of the porous layer. The value of EOT was determined by the Fourier transformation of the reflectance spectra calculated with the IGOR program (Wavemetrics, Inc.). Fourier transformation resulted in a sharp peak whose position was equal to the product value of $2nL$ in Eq. (1). The method for detecting optical thickness described herein is actually FT-RIFS.

2.3. Construction of Au–PSi DNA sensor

The synthetic 22-mer probe and target ODNs were purchased from the Shanghai SBS Genetic Tech Co. (China). The sequence of the probe DNA was 5-thiol-CTA CAG GTG AAG GTG GAA TGG T, and the target DNA sequence was GAT GTC CAC TTC CAC CTT ACC A, which is complementary to the probe DNA. For the DNA sensor fabrication, the probe DNA was dissolved in 50 mM Tris–HCl–EDTA buffer (pH 7.4) to make a 10 μmol L^{-1} of solution. A 10 μL aliquot of thiolated probe ssDNA solution was dropped onto the Au–PSi chip and incubated for 6 h. After the immobilization of the probe ssDNA, the free DNA was washed away by immersing the chip in an ultrasonic bath filled with distilled water. After drying the chip on a hot plate (40 °C), the EOT value of the Au–PSi attached with ssDNA was detected by the methods described in the Section 2.2.

To realize multiple detections and ensure the repeatability of the optical detection on the same Au–PSi chip, the sensing area exposed to the sample solution was defined by a patterned polydimethylsiloxane (PDMS) membrane. Arrays of holes with diameters of approximately 1.0 mm arranged in an orderly 3 × 3 pattern were punched on a thin layer of PDMS membrane. The surfaces of the PDMS membrane and silicon chip adhered to each other after both of them were treated with oxygen plasma for 2 min. The probe ssDNA was attached to the wall of the nanoporous channel of each sensing spot with the same methods described above. A 10 μL aliquot of the target ODN solution with different concentrations was then dropped onto each Au–PSi sensing spot, which was incubated for 2 h. Thereafter, the free ODNs were washed away by ultrasonication. The EOT value of each sensing spot before and after the DNA hybridization was detected by FT-RIFS, respectively, and the shift in EOT was calculated. All the optical detection was performed after the sensing spots were dried in air. The control experiment was conducted by the same methods, but the target ODN was replaced with 10 μmol L^{-1} of non-complementary ssDNA (CTA GTG AAG GTG GAA CAG TGG T). The instrumental setup and mechanism for optical detection are depicted in Scheme 1.

2.4. Electrochemical measurements

Electrochemical impedance spectroscopy (EIS) was measured on an Autolab system (Metrohm, Switzerland), in which the Au–PSi was used as a working electrode. EIS was performed in a 0.01 M Tris–HCl (pH 7.4) buffer solution containing 1.0 mmol L^{-1} EDTA, 0.1 mmol L^{-1} $Fe(CN)_6^{4-}/Fe(CN)_6^{3-}$ redox couple, and 0.1 M KNO_3. A 5 mV amplitude sine wave was applied to the electrode at the

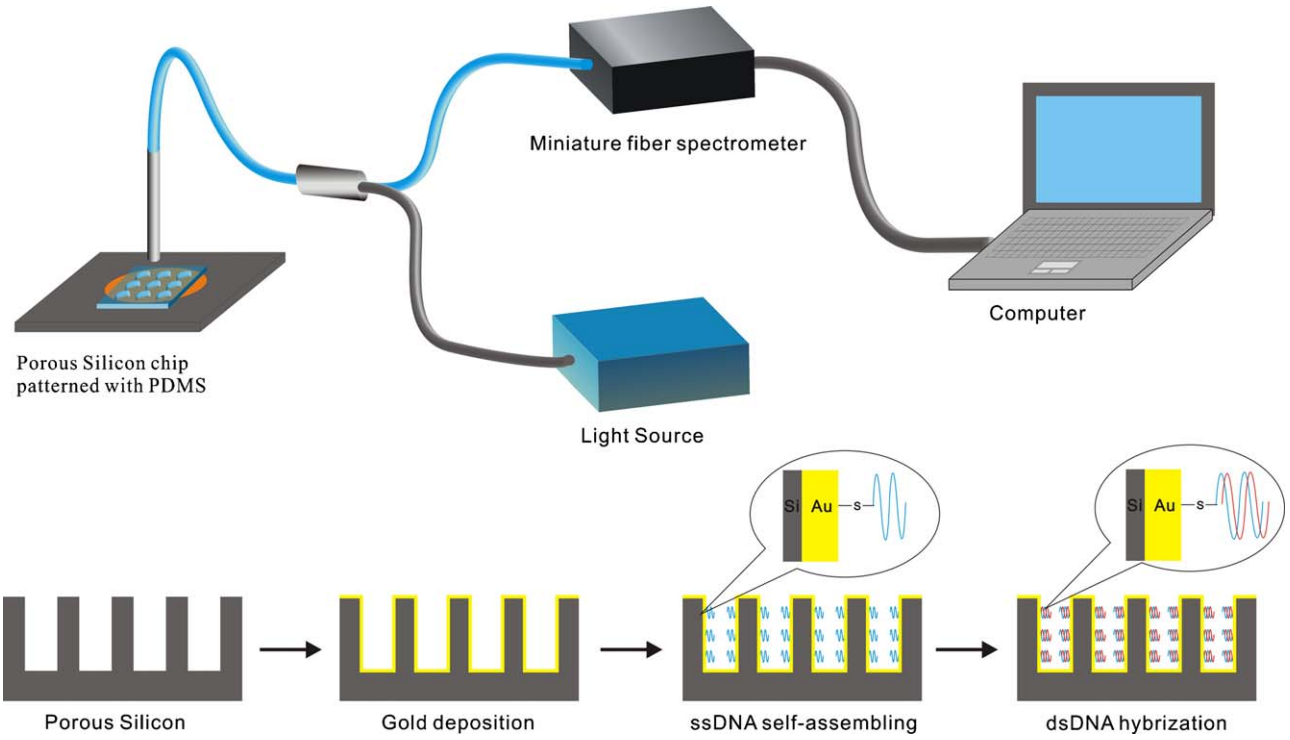

Scheme 1. (a) Experimental setup for the optical detection. (b) Procedure for the preparation of nanoporous gold arrays, ssDNA attachment, and target ODN hybridization.

formal potential of the redox couple with a frequency range from 0.01 Hz to 100 kHz.

3. Results and discussion

3.1. Surface morphology characterization of Au–PSi

The surface morphology of the PSi chip partially coated with gold atoms was revealed in the top side view of the SEM image (Fig. 1a). The average diameter of the silicon nanopores was approximately 20 nm before Au deposition. After the Au layer deposition, the radius of the nanopore was reduced to approximately 11 nm, and the porous structure was retained perfectly. In fact, the diameter of gold nanopore varied with the change of conditions for electrodeposition, such as time, concentration of $H[AuCl_4]$, as well as the electrolysis current. Thus, controlling the diameter of nanoporus gold can be realized. Meanwhile, the surface morphology of Au–PSi was also significantly dependent on these electrodeposition parameters. At high deposition currents or $HAuCl_4$ concentrations, large amount of nano/micro gold particles was observed on the surface of Au–PSi. The porous structure even disappeared when the whole porous area was filled with gold particles. Similar "pore filling" phenomena had also been observed when a macroporous silicon template was used (Aravamudhan et al., 2007; Fukami et al., 2008). For label free optical detection, metal deposition at the pore opening layer or in a "pore filling" way should be avoided, since the porous structure will be destroyed and surface area dramatically decreases. Moreover, the interference fringe in the reflectance spectra will also disappeared, because the gold particles filling in the pore channel or depositing at the pore opening layer may prevent light from penetrating into the interface of the porous layer and bulk silicon. Using a decreased electrodeposition current and low concentration of $HAuCl_4$, formation of nano/micro gold particles was inhibited, and the nanoporous gold arrays showing similar physical structure and optical properties to PSi was obtained. A previous study suggested that the deposition of Au atoms on porous anodic alumina (PAA) by thermal evaporation method may form a "gold cap" on the top of the PAA layer (Kim et al., 2007). However, from the cross-sectional view of SEM image (Fig. 1b and c), we can deduce that the gold nanolayer may be deposited throughout the pore channel surface, since the surface morphology of the whole channel obviously changed. This can also be confirmed by electrochemical impedance measurements conducted and discussed in subsequent sections.

3.2. Comparison of the reflectance spectra of PSi and Au–PSi

The spectrum of the Au–PSi chip also exhibited well-defined Fabry–Pérot fringes, which are similar with the PSi fringes, except that the peaks of the fringes shifted to a new position (Fig. 2a). The white light reflected from the interface of air/PSi and PSi/bulk silicon resulted in an interference pattern related to the thickness (L) and the refractive index (n) of the film, as described in Eq. (1). The fast Fourier transform (FFT) spectra of PSi and Au–PSi are shown in Fig. 2b. Compared with PSi, a significant blue shift in the optical thickness was found in the FFT spectrum of Au–PSi. The decrease in the optical thickness of the porous layer can be explained by the Bruggman equation. Usually, the Bruggman dielectric constant approximation [Eq. (2)] (Astrova and Tolmachev, 2000) can be used to calculate the effective dielectric constant of the PSi layer:

$$(1-f)\frac{\varepsilon_{Si}-\varepsilon_{eff}}{\varepsilon_{Si}+2\varepsilon_{eff}}+f\frac{\varepsilon_{air}-\varepsilon_{eff}}{\varepsilon_{air}+2\varepsilon_{eff}}=0 \quad (2)$$

f denotes the pore fractions in the porous layer. ε_{Si} and ε_{air} represent the dielectric functions of silicon and air, respectively. After the gold film electrodeposition, the porous layer can be regarded as a homogeneous dielectric material composed of air, silicon, and gold. This is because the pore dimensions of the porous layer are far less than the incident light wavelength. Accordingly, the effective

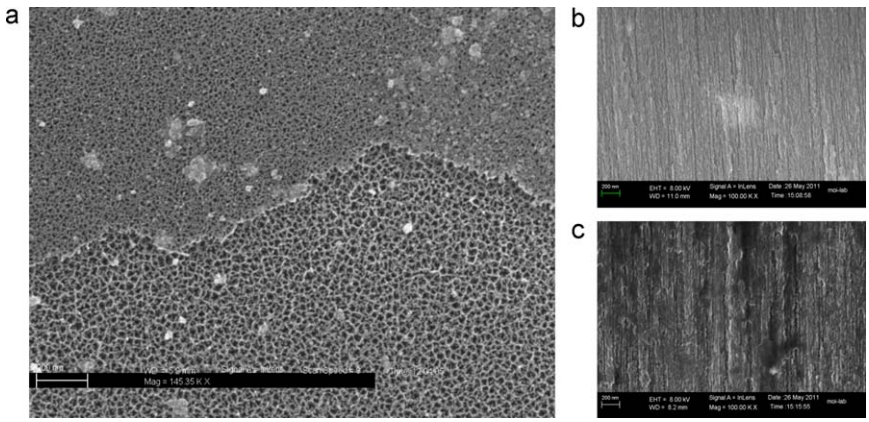

Fig. 1. (a) Scanning electron micrograph (SEM) of porous silicon (PSi) and nanoporous gold on the PSi template (Au–PSi). To compare the surface morphology of PSi and Au–PSi, a part of the etched area on the PSi wafer was masked with a plastic adhesive tape before the electrodeposition process. The tape was peeled off to expose the uncoated area before the SEM scanning was performed. (b) Cross-sectional SEM image of PSi. (c) Cross-sectional SEM image of Au–PSi.

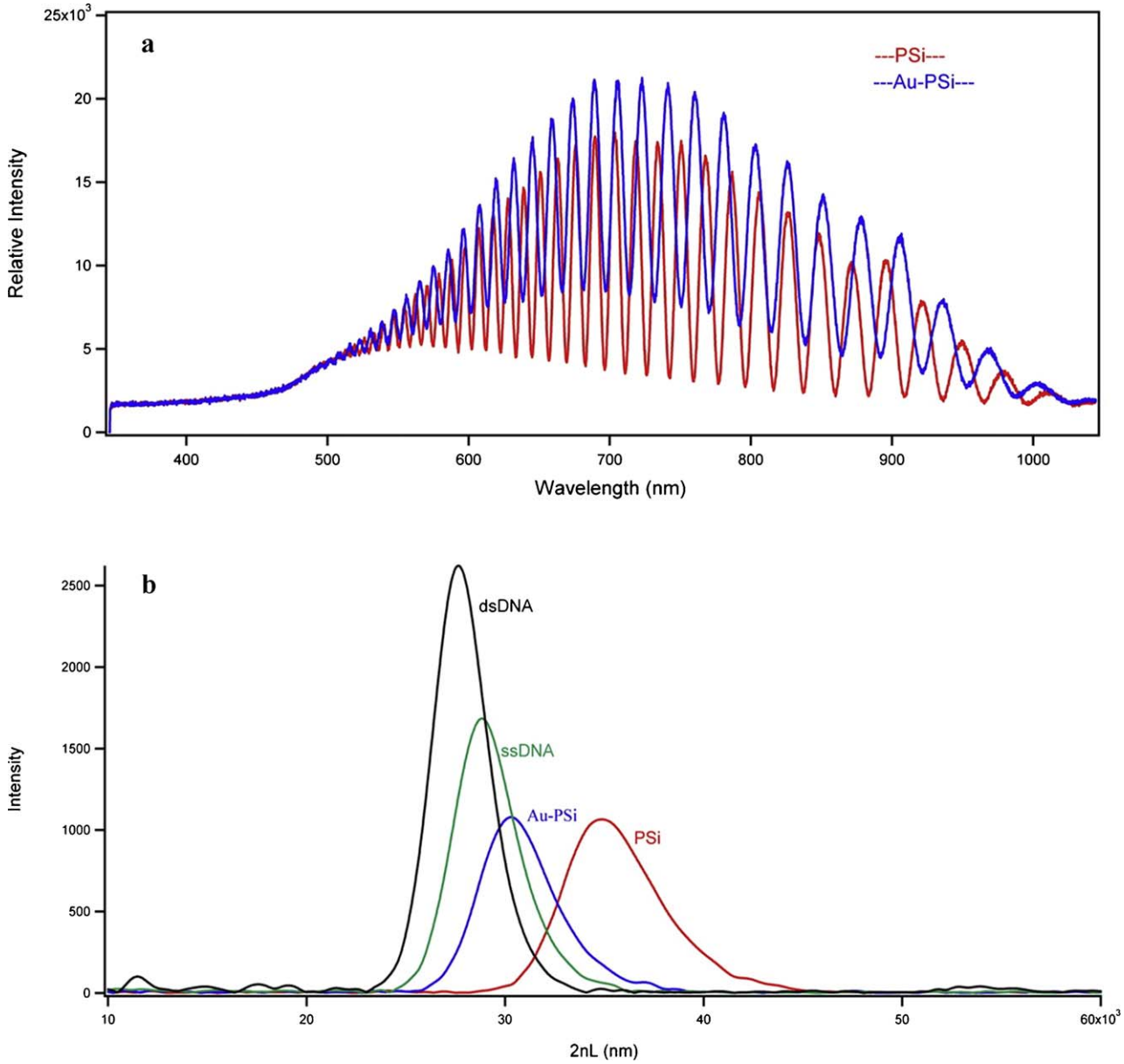

Fig. 2. Relative reflectance and Fourier transform spectra of the porous substrate. (a) Relative reflectance spectra of PSi and Au–PSi at an integration time of 100 ms. (b) Fourier transform reflectometric interference spectra of PSi, Au–PSi, Au–PSi attached with ssDNA, and the one subsequently incubated with target ODNs to form dsDNA in the pore channels.

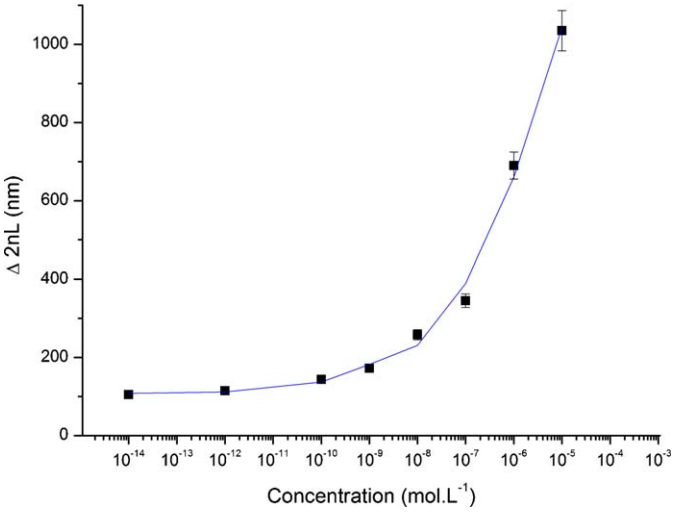

Fig. 3. Relationship between the optical thickness shift of the nanoporous layer and the concentration of the target ODN molecules. Each data was an average value of replicated measurements ($n = 3$).

refractive index (n_{eff}) of the porous layer can be expressed by Eq. (3):

$$(1-f)\frac{n_{Si}^2 - n_{eff}^2}{n_{Si}^2 + 2n_{eff}^2} + (f-V)\frac{n_{air}^2 - n_{eff}^2}{n_{air}^2 + 2n_{eff}^2} + V\frac{n_{Au}^2 - n_{eff}^2}{n_{Au}^2 + 2n_{eff}^2} = 0 \quad (3)$$

V represents the volume fraction of gold in the porous layer. n_{Si}, n_{air}, and n_{Au} denote the refractive indices of silicon, air, and gold, respectively. Given that n_{Au} is less than both n_{Si} and n_{air}, solving Eq. (3) reveals that n_{eff} of the whole porous layer decreases. This trend led to the blue shift in the $2nL$ value.

3.3. Optical response and performance of Au–PSi DNA biosensor for the detection of ODNs

As shown in Fig. 2b, the $2nL$ value of the porous layer continued to decease after Au–PSi was attached to the thiolated probe ssDNA (5-thiol-CTA CAG GTG AAG GTG GAA TGG T). The detection of target ODNs was realized by subsequently monitoring the $2nL$ value after the chip was exposed to target ODNs, with their sequences fully complementary to the probe ssDNA. The optical measurement results show that the $2nL$ value further blue shift after the hybridization of target ODNs. Fig. 3 indicates that the blue shift of the optical thickness increased with the exponential increase of ODN concentration. However, the optical signal responding to a high concentration ODNs did not show a saturated respond as expected in most sensor behaviors. We attribute this phenomenon to the extremely high surface area of the nanoporous gold array, which provided more sites for attaching a large number of probe ssDNAs. Consequently, the dynamic range responding to target ODNs molecules significantly increased. The lowest ODN concentration measured with the nanoporous gold array was estimated at around 10^{-14} mol L^{-1}. As we know, the limit of detection (LOD) depends on the variability of the baseline noise. In our experimental conditions, a variation of ~5 nm in the value of EOT was found in the blank assay. A lower LOD value could be achieved if the baseline noise decreased. To exclude the possibility of nonspecific interactions, non-complementary ssDNA (CTA GTG AAG GTG GAA CAG TGG T; 10^{-5} mol L^{-1}) was applied onto the same Au–PSi chip. The optical signal was detected by the same procedure. As expected, the change in the 2 nL value was almost the same as what was observed in blank assay ($n = 5$, $P = 0.95$). The results indicated that the nonspecific adsorption of ODN is negligible. Detection by nanoporous devices may show additional selectivity compared with other kinds of sensing materials. This selectivity is attributed to the fact that nanopores only allow small molecules, such as ODNs, to penetrate the sensing layer. Therefore, large DNA molecules, even those containing the same complementary fragments, cannot interfere with the OND detection, since these large molecules will be excluded by the nanopore structure. However, interference from small molecules with mercapto group cannot be eliminated, because they have a high affinity for the gold surface.

In addition, Au–PSi had a high chemical stability. The optical signal responding to the same ODN concentration did not show an observable change even after the Au–PSi chip was stored in a phosphate-buffered saline for 3 months. The relative stability of the Au–PSi chip should be owed to the protective effect of the gold nanolayer on PSi. The advantages of PSi-templated nanoporous gold arrays may not only be its high stability. Surface functionalizations on the porous gold arrays can be conveniently realized via the self-assembly of thiolated molecules. Moreover, the porous gold arrays can potentially act as a new kind of electrode for electrochemical analyses for observing the binding events in nanopore structures.

3.4. Mechanistic study of the optical response

Apparently, the decreased refractive index n of the nanoporous layer on the binding of biomolecules was responsible for the optical response. However, this phenomenon cannot be explained by the Bruggman theory because the refractive index of ODNs is larger than air. On the other hand, the electromagnetic theory can explain the decrease in n caused by the DNA attachment and hybridization in the wall of Au–PSi. The Maxwell theory states that the refractive index of a substance is directly related to its effective dielectric constant, as expressed by Eq. (4) (Stratton, 2007):

$$n_{eff} = \varepsilon_{eff}^{1/2} b \quad (4)$$

where n_{eff} and ε_{eff} represent the effective refractive index and effective dielectric constant, respectively. We deduced that the DNA molecular assembly on the inner wall of the gold nanopores may have affected the interfacial capacitance, and subsequently changed the effective dielectric constant of the layer.

The interfacial capacitance of the nanoporous gold channel attached with ssDNA can be regarded as a series capacitance combination (C_1) comprising the capacitances of gold-coated silicon (C_0) and DNA (C_2) layers that self-organized on the channel surface. The relationship between these capacitances can be expressed by Eq. (5):

$$\frac{1}{C_1} = \frac{1}{C_0} + \frac{1}{C_2} \quad (5)$$

Before the attachment of ssDNA, C_1 was equal to C_0. According to Eq. (5), C_1 will decrease after introducing a probe ssDNA layer self-assembled on the channel wall.

The DNA layer attached on the gold channel surface can be regarded as a parallel plate capacitor, whose capacitance is given by Eq. (6):

$$C_2 = \varepsilon_0 \varepsilon \frac{A}{L} \quad (6)$$

ε is the relative dielectric constant of the DNA layer and ε_0 is the vacuum dielectric constant. A represents the surface area of the channel wall attached with DNA, and L represents the thickness of the DNA layer. Accordingly, changes in the DNA layer thickness cause changes in C_2.

Although the Au–S bond is vertical to the gold surface, the spatial structure of ssDNA in its bent form is prone to lie on the wall of nanoporous channels. After this ssDNA is hybridized to the target, a more rigid double-stranded DNA (dsDNA) formed. This event

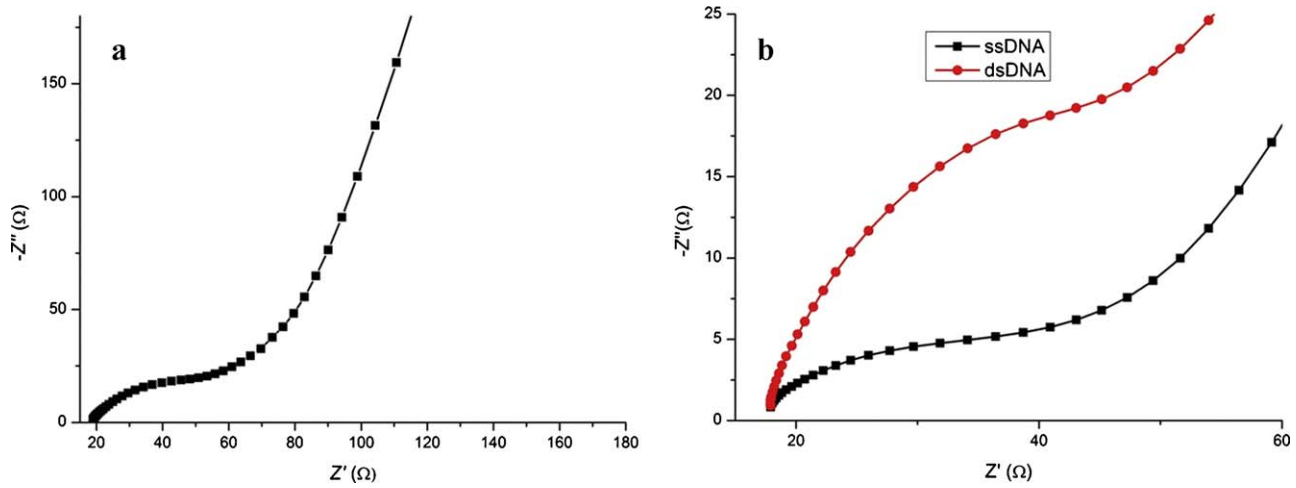

Fig. 4. (a) The entire electrochemical impedance plot for a nanoporous Au–PSi electrode attached to ssDNA. (b) Magnified electrochemical impedance plot in a high frequency range before and after the target ODN hybridization on the ssDNA attached to the Au–PSi electrode.

occurred because the double DNA strain repelled each other via electrostatic forces and elongated the DNA chain (Herne and Tarlov, 1997). According to Eqs. (5) and (6), an increase in L decreases the capacitance of the DNA layer (C_2), and consequently cause a further decrease in C_1 and in the effective refractive index of the nanoporous layer. The decrease in C_1 was also confirmed by EIS. This method is effective in determining the interface properties of surface-modified electrodes (Orazem and Tribollet, 2006). As shown in Fig. 4a, the impedance plot of the nanoporous gold electrode attached with the ssDNA comprised a semicircle-shaped portion at high frequencies. This portion corresponded with the electron transfer limiting process. A linear portion observed at lower frequencies resulted from the diffusion-limiting step of the electrochemical process. The appearance of the semicircle portion at high frequencies indicated the blocking behavior of the ssDNA attached on the nanoporous gold surface to the redox couple. For the bare gold electrode, a large electron transfer rate constant of the redox couple resulted in only a unit-sloped Warburg line. Therefore, the electrochemical impedance plot shown in Fig. 4 can be regarded as a signal for confirming the existence of an electrical double layer after the attachment of ssDNA to the inner surface of the nanoporous gold arrays. After hybridizing the target and probe ssDNAs, the diameter of the semicircle portion on the impedance plot significantly elevated (Fig. 4b). This finding demonstrated that as the dsDNA formed, electron transfer resistance increased with decreased effective electrode area or increased insulator thickness (Mearns et al., 2006). From an electrochemical perspective (Orazem and Tribollet, 2006), the increased impedance indicated a decreased interfacial capacitance and consequently a decreased dielectric constant. This relationship verified the assumption we deduced from the optical detection results. Fig. 4 shows that the electrochemical impedance of the Au–PSi electrode was significantly lower than common macroscopic gold electrode probably because of the large surface area of the nanoporous gold electrode. Accordingly, the EIS data not only explained the optical responding behavior of Au–PSi, but also verified that the gold atom was deposited on the inner surface wall of the PSi. Consequently, a high surface area for biological sensing was provided.

4. Conclusions

We demonstrated that nanoporous gold arrays can be conveniently and controllably obtained by the electrodeposition of gold layers on well-ordered nanoporous PSi films. A label-free optical DNA sensor for ODN detection can be successfully constructed by attaching the thiolated probe ssDNA on the inner surface of Au–PSi. Molecular binding events in Au–PSi can be optically detected, based on a shift of the EOT value, as monitored by FT-RIFS. In combination with the advantages of gold and PSi, the fabricated Au–PSi sensor showed high sensitivity, good chemical stability, as well as surface properties that can be conveniently tailored by a variety of self-assembled monolayers via thiol chemistry. Moreover, due to the good conductivity and well controlled pore diameter of Au–PSi, it can also potentially act as novel porous electrode, which will find numerous applications in electrobiosensor. The present study will lead us to develop our future work concerning with the switchable nanopore sensor for genetic testing, drug discoveries, and other applications in the bioanalytical field.

Acknowledgements

The authors acknowledge the financial support of the National Science Foundation of China (NFSC) under grant number 21075111.

References

Aravamudhan, S., Luongo, K., Poddar, P., Srikanth, H., Bhansali, S., 2007. Appl. Phys. A 87, 773–780.
Astrova, E.V., Tolmachev, V.A., 2000. Mater. Sci. Eng., B 69–70, 142–148.
Chan, S., Horner, S.R., Fauchet, P.M., Miller, B.L., 2001. J. Am. Chem. Soc. 123 (47), 11797–11798.
Cunin, F., Schmedake, T.A., Link, J.R., Li, Y.Y., Koh, J., Bhatia, S.N., Sailor, M.J., 2002. Nat. Mater. 1 (1), 39–41.
Dancil, K.-P.S., Greiner, D.P., Sailor, M.J., 1999. J. Am. Chem. Soc. 121 (34), 7925–7930.
Fukami, K., Kobayashi, K., Matsumoto, T., Kawamura, Y.L., Sakka, T., Ogata, Y.H., 2008. J. Electrochem. Soc. 155, D443–D448.
Garcia-Maldonado, M.D., Rosario-Canales, M.R., Guadalupe, A.R., 2005. Abstr. Paper Am. Chem. Soc. 229, 313–320.
Herne, T.M., Tarlov, M.J., 1997. J. Am. Chem. Soc. 119 (38), 8916–8920.
Hong, C., Kim, H., Park, S., Lee, C., 2010. J. Eur. Ceram. Soc. 30 (2), 459–463.
Kececi, K., Sexton, L.T., Buyukserin, F., Martin, C.R., 2008. Nanomedicine 3 (6), 787–796.
Kim, D.-K., Kerman, K., Saito, M., Sathuluri, R.R., Endo, T., Yamamura, S., Kwon, Y.-S., Tamiya, E., 2007. Anal. Chem. 79 (5), 1855–1864.
Lin, V.S.Y., Motesharei, K., Dancil, K.-P.S., Sailor, M.J., Ghadiri, M.R., 1997. Science 278 (5339), 840–843.
Martin, C.R., Siwy, Z.S., 2007. Science 317 (5836), 331–332.
Mearns, F.J., Wong, E.L.S., Short, K., Hibbert, D.B., Gooding, J.J., 2006. Electroanalysis 18 (19–20), 1971–1981.

Orazem, M.E., Tribollet, B., 2006. Electrochemical Impedance Spectroscopy. Wiley InterScience, New York.
Rong, G., Najmaie, A., Sipe, J.E., Weiss, S.M., 2008a. Biosens. Bioelectron. 23 (10), 1572–1576.
Rong, G.G., Ryckman, J.D., Mernaugh, R.L., Weiss, S.M., 2008b. Appl. Phys. Lett. 93 (16), 3.
Stein, C.A., Cohen, J.S., 1988. Cancer Res. 48 (10), 2659–2668.
Stratton, J.A., 2007. Electromagnetic Theory. Wiley-IEEE Press, Hoboken.
van Noort, D., Mandenius, C.-F., 2000. Biosens. Bioelectron. 15 (3–4), 203–209.
Wirtz, M., Martin, C.R., 2003. Adv. Mater. 15 (5), 455–458.